Yeast cells depleted of the frataxin homolog Yfh1 redistribute cellular iron: studies using Mössbauer spectroscopy and mathematical modeling

Salvador Fernandez^{1,#}, Joshua D. Wofford^{2#}, Rachel E. Shepherd^{1#}, Shaik Waseem Vali³, Andrew Dancis⁴, and Paul A. Lindahl^{1,3}*

¹From the Department of Chemistry, Texas A&M University, College Station Texas 77843-3255. 2. Department of Chemistry, College of Science and Mathematics, Charleston Southern University, Charleston South Carolina, 29406. 3. Department of Biochemistry and Biophysics, Texas A&M University, College Station Texas 77843. 4. Department of Medicine, Division of Hematology-Oncology, Perelman School of Medicine, University of Pennsylvania, Philadelphia, PA 19104, USA.

Running title: Cellular iron redistribution in Yfh1-deficient yeast

*To whom corresponding should be addressed: Paul A. Lindahl, Department of Chemistry, Texas A&M University, College Station TX 77843-3255. Phone, 979-845-0956; Fax, 979-845-4719, email: lindahl@chem.tamu.edu.

Keywords: Electron paramagnetic resonance; iron trafficking and regulation; ordinary differential equations; mitochondria; vacuoles; cytosol.

ABSTRACT

The neurodegenerative disease Friedreich's Ataxia arises from a deficiency of frataxin, a protein that promotes iron-sulfur cluster (ISC) assembly in mitochondria. Here, primarily using Mössbauer spectroscopy, we investigated the iron content of a yeast strain in which expression of Yeast Frataxin Homolog 1 (Yfh1), oxygenation conditions, iron concentrations, and metabolic modes were varied. We found that aerobic fermenting Yfh1-depleted cells grew slowly and accumulated Fe^{III} nanoparticles, unlike WT cells. Under hypoxic conditions, the same mutant cells grew at rates similar to WT cells and had similar iron content, and were dominated by Fe^{II} rather than Fe^{III} nanoparticles. Furthermore, mitochondria from mutant hypoxic cells contained approximately the same levels of ISCs as

WT cells, confirming that Yfh1 is not required for ISC assembly. These cells also did not accumulate excessive iron, indicating that iron accumulation into yfh1-deficient mitochondria is stimulated by O2. In addition, in aerobic WT cells, we found that vacuoles stored Fe^{III}, whereas under hypoxic fermenting conditions, vacuolar iron was reduced to Fe^{II}. Under respiring conditions, vacuoles of Yfh1-deficient cells contained Fe^{III}, and nanoparticles accumulated only under aerobic conditions. Taken together, these results informed a mathematical model of iron trafficking and regulation in cells that could semi-quantitatively simulate the Yfh1-deficiency phenotype. Simulations suggested partially independent regulation in which cellular iron import is regulated by ISC activity in mitochondria, mitochondrial iron import is regulated by a mitochondrial

^{*}Equal contributions.

 Fe^{II} pool, and vacuolar iron import is regulated by cytosolic Fe^{II} and mitochondrial ISC activity.

Introduction

Humans suffering from Friedreich's Ataxia are deficient in *frataxin* (1). This protein binds a multi-protein complex in the mitochondrial matrix that catalyzes assembly of iron-sulfur clusters (ISCs) (2). Yeast frataxin homolog 1 (Yfh1) in Saccharomyces cerevisiae acts similarly, which allows budding yeast to serve as a workhorse for probing the pathogenic mechanism of this disease. Frataxin binds cysteine desulfurase, a member of this complex, which stimulates the rate by which a sulfur atom is extracted from free cysteine and transferred to the scaffold. Once coordinated to iron and reduced by ferredoxin (Yah1), this sulfur becomes the bridging sulfide of a [Fe₂S₂]²⁺ cluster bound to the Isu1/2 scaffold proteins (3). Δ Yfh1 yeast cells grown under aerobic conditions deficient mitochondrial ISCs and heme centers, as well as other phenotypic properties that are less easily interpreted (4-7). For example, Yfh1 protects cells against oxidative stress (8).

Fermenting aerobic $\Delta Y fh1$ yeast cells import excessive amounts of iron which flows into mitochondria and reacts to form Fe^{III} nanoparticles (5,6). The iron concentration of mitochondria in which nanoparticles have accumulated is 10-15 fold higher than in the WT organelle (4,9). This accumulation indicates iron dysregulation. Fermenting ΔYfh1 cells grow slowly relative to WT cells and are more easily damaged by O2 and other reactive oxygen species (ROS) (10). How these properties are causally related at the molecular incompletely understood. level remains Understanding these relationships, the longterm goal of this study, may reveal better approaches for treating the disease.

The model of Fig. 1 describes our current understanding of these relationships, as

supported by Mössbauer-based data presented here. First some background.

[Insert Fig. 1]

In our study, IRON refers to ⁵⁷Fe^{III} citrate which we added to growth media (note: nutrients are capitalized). IRON is typically imported into the cell through the Fet3 transport system on the plasma membrane (11,12). However, under hypoxic conditions, the Fet4 importer is used. Imported iron ultimately generates the cytosolic labile Fe^{II} pool (13), called **FC** in the model (note: model components are bold when introduced).

Vacuoles are acidic organelles that reversibly store iron. Under iron-replete conditions, they import FC via the membrane-bound transporter Ccc1 (14). Imported Fe^{II} in vacuoles (**F2** in the model), is rapidly oxidized to form Fe^{III} polyphosphate complexes, **F3** (16-18). F3 can be converted to vacuolar nanoparticles (**VP**) (15).

Some FC is converted into CIA, a model component representing all iron species in the cytosol, nucleus, and endoplasmic reticulum except for FC. CIA includes [Fe₄S₄]-containing proteins that are synthesized by the <u>Cytosolic Iron-sulfur cluster Assembly system.</u>

Much FC is trafficked into mitochondria through two paralogous high-affinity Fe^{II} importers (Mrs3 and Mrs4) on the inner membrane (16,17). Iron entering mitochondria forms an Fe^{II} pool (18,19), referred to as **FM**, which serves as substrate for the biosynthesis of mitochondrial ISC and hemes, collectively symbolized as **FS**. Yfh1 is presumed to be a catalyst for the FM \rightarrow FS reaction; the same reaction is inhibited by mitochondrial component **O2**.

Understanding the cell's response to Yfh1 deficiency requires understanding how genes involved in iron homeostasis are regulated (indicated by the red circles and dashed lines in Fig. 1). The *Iron Regulon* includes a few dozen genes whose expression is controlled by Aft1 and Aft2 (20-22). These paralogous transcription factors regulate: a) iron import

into the cell; b) iron import into mitochondria (23); and c) iron export from vacuoles into the cytosol. Thus, iron export from vacuoles to cytosol is commonly thought to be regulated like the import of nutrient iron into cytosol (24).

Other systems help regulate iron homeostasis in the cell. Besides Aft1/2, Fet4 expression is regulated by O₂ (24). Under iron-replete conditions, vacuolar iron import through Ccc1 is positively regulated by Yap5, another ironsensing transcription factor (25), as well as by cellular stress factors. Under iron-starved conditions, Cth1 and Cth2 mediate degradation of Ccc1 mRNA (26). Other regulatory factors add further complexity to understanding regulation (27-29).The generation mitochondrial nanoparticles (MP), loss of ISC activity, and excessive oxidative damage are major cellular responses to Yfh1 deficiency (7,29-31).

One strategy for disentangling the confounding effects of O2 is to minimize its exposure to Δ Yfh1 cells (16,30,32,33). Hypoxic conditions are more useful than rigorously anaerobic ones because low concentrations of O2 are required for heme biosynthesis. ΔYfh1 cells grow slowly under aerobic conditions but faster under hypoxic ones. When grown hypoxically on YPAD, Δ Yfh1 cells exhibit no obvious phenotype (32) except for low aconitase activities (30). Aconitase is used as a reporter of ISC assembly activity because it requires an [Fe₄S₄] cluster for activity. Aerobic fermenting ΔYfh1 cells lack aconitase activity, so the presence of ISCs in the same cells grown hypoxically suggests that *Yfh1* is not required for ISC biosynthesis.

Frataxin also minimizes oxidative stress. When anaerobic $\Delta Y fh1$ and WT cells are exposed to air, oxidative damage to $\Delta Y fh1$ cells increases. However, ISC-containing ferredoxin is quite stable inside $\Delta Y fh1$ mitochondria (32,34) suggesting that O₂ inhibits ISC biosynthesis.

The Respiratory Shield hypothesis (35-37) forms the core of the Fig. 1 model. It assumes that the mitochondrial matrix of healthy WT cells grown under aerobic conditions is largely devoid of O2 due to respiratory activity on the inner membrane. In WT cells, the shield protects FM from reacting with O2. In the absence of Yfh1 or other proteins involved in ISC assembly or trafficking, the reaction FM \rightarrow FS is slowed, which slows the rate of O₂ reduction by the respiratory complexes. This allows more O₂ to diffuse into the matrix region where it reacts with FM to form MP, thereby limiting the amount of FM available as a substrate for FS. This weakens the respiratory shield and initiates a vicious cycle in which the further decline of FM further slows the synthesis of FS and the rate of respiration. The lack of FS activates the iron regulon which increases iron import into the cell and mitochondria. The net effect is mitochondria spiral down into a diseased state in which: a) the organelle is filled with nanoparticles; b) both ISC and heme activities are low; and c) O2 and ROS flood the cell.

Similar accumulations of nanoparticles in mitochondria are observed for other genetic strains of yeast harboring defects in ISC biosynthesis or trafficking including cells deficient in Yah1 (31), Ggc1 (6), Atm1 (33), and Ssq1 (6). Even more surprising is that a similar phenotype is observed in strains with mutations that are not primarily involved in either ISC assembly or trafficking. This includes cells deficient in Mtm1 (38) and cells in which the Aft1 transcription factor is constitutively up-regulated (39). Thus, iron dysregulation appears to be a secondary response to defects in various mitochondrial processes including but not limited to ISC assembly, trafficking and/or regulation. The Respiratory Shield hypothesis can explain these diverse causes, since the strength of the shield reflects processes such as respiration, bioenergetics, and mitochondrial membrane potential in which many proteins contribute.

Mitochondria from $\Delta Y fh1$ yeast cells (reportedly) do *not* accumulate excessive iron when they respire (40). Moreover, aconitase activities in respiring $\Delta Y fh1$ cells are $\sim 70\%$ of WT levels whereas they are near zero in aerobic fermenting $\Delta Y fh1$ cells. Understanding these metabolic differences might reveal new insights into the mechanism of the disease.

For this study, we primarily used Mössbauer spectroscopy to probe the relationships giving rise to the Yfh1-deficiency phenotype. We investigated a strain of yeast in which Yfh1 expression is dictated by the estradiol concentration in the growth medium (6,41). This strain allowed us to probe the effects of gradually reducing the expression of Yfh1. We also examined the effects of O2, nutrient iron, and metabolic mode on cellular iron content. We evaluated the iron content of mitochondria from anaerobic fermenting and respiring Yfh1deficient cells grown under hypoxic conditions. We then used those and other results to develop the model of Fig. 1, and then used the model to simulate the yfh1-deficient phenotype. Our results offer new insights into the pathogenesis of Friedreich's Ataxia.

Results

We employed the mutant strain ERyfh1 in this study because the expression level of Yh11 could be varied according to the concentration of estradiol [EST] added to the growth medium (6,41). As expected, Yfh1 was undetectable in a Western blot of soluble lysates from cells grown in the absence of estradiol ([EST] = 0), and expression increased as [EST] increased (Fig. 2).

[Insert Fig. 2]

The [EST] required for full expression was higher than that reported by Seguin et al. (6,41). They reported that [EST] > 10 nM was sufficient to generate WT expression levels of Yfh1 whereas our samples required roughly 1000 nM [EST] to exhibit WT properties.

We used a shorthand nomenclature to describe the growth conditions for various

experiments. <u>A</u>erobic <u>F</u>ermenting <u>W</u>ild-Type (<u>AFW</u>) cells cultured in glucose-containing minimal medium (MM) grew in accordance with an exponential growth rate $\alpha \approx 0.2$ - 0.3 hr⁻¹ where α is the linear slope of ln(OD600) vs time plots (Table S1). Aerobic fermenting mutant cells (<u>AFM</u>) grew at similar rates ($\alpha \approx 0.2 \text{ hr}^{-1}$) at [EST] > ~25 nM but slower at [EST] = 0. Supplementing media with Fe^{III} citrate at concentrations between 1 \rightarrow 100 μ M had no effect on growth rate. WT cells cultured on 1 μ M Fe^{III} citrate grow at rates comparable to those of iron-replete WT cells (19).

Aerobic fermenting mutant cells grown in media containing [EST] = 0 and [IRON] = 40will be called AFM0-40 cells, where the first number refers to the nM concentration of EST and the second to the µM concentration of Fe^{III} citrate. Both are final concentrations in the growth media. WT cells averaged ~ 600 µM iron, similar to reported values (18). The iron concentration AFM0-40 of cells significantly higher than that of AFW-40 cells (Table S1). The relative intensities of the MB spectra (see below) confirmed that AFM0-40 cells were iron-overloaded.

AFM0 cells contained ca. $500-1800~\mu M$ Fe depending on growth media. As [EST] increased, the cellular iron concentration declined, eventually reaching concentrations typical of WT cells. This supports the observed decline in MB spectral intensities as [EST] increased (see below). The similar iron concentrations obtained under these conditions suggested that AFM cells expressing WT levels of Yfh1 were *not* iron-dysregulated, as expected.

When grown under hypoxic conditions, both fermenting WT and mutant cells (called HFW and HFM cells, respectively) grew in accordance with $\alpha \approx 0.2~hr^{-1}$ regardless of [EST] or [IRON]. The concentration of iron in mutant cells under hypoxic conditions was comparable to that of WT cells (Table S1). Under hypoxic conditions, mutant cells were not noticeably dysregulated.

[Insert Fig. 3]

Mössbauer (MB) spectra of AFM cells grown with different [EST]: We used MB spectroscopy to investigate how the iron content of the mutant cells changed as the [EST] decreased. As expected, AFM1000-40 cells exhibited MB spectra typical of WT (W303) cells (compare Fig. 3A to Fig. 1D of Ref 18). Spectral features included: a) a magnetic feature arising from vacuolar NHHS Fe^{III} polyphosphate (brown line); b) a *Central* Doublet (CD) arising from [Fe₄S₄]²⁺ clusters and LS Fe^{II} hemes combined (green line); and c) two minor doublets arising from nonheme high-spin (NHHS) Fe^{II} (dark blue line) and HS Fe^{II} hemes (light blue). Some CD originated from mitochondrial iron while the remainder arose mainly from [Fe₄S₄]²⁺ clusters in the cytosol and nucleus. A low-intensity doublet likely due to nanoparticles (magenta) was also present. Percentages used decompositions are in Table S2.

When [EST] was lowered to 100 nM, spectral intensity due to vacuolar NHHS Fe^{III} declined while that of the NHHS Fe^{II} doublet increased (Fig. 3B). AFM25-40 and AFM0-40 spectra were essentially devoid of the HS Fe^{III} feature. A relatively intense NHHS Fe^{II} doublet was evident in all spectra between AFM100-40 → AFM0-40. A minor shoulder on the inside edge of the low-energy line of this doublet (see arrow) probably arose from the CD (represented as the sum of FS + CIA in the model) but resolution was limited. According to the model of Fig. 1, the early loss of vacuolar NHHS Fe^{III} (F3 in the model) indicates that the earliest titration event that occurs as Yfh1 levels decline is the reduction of F3 \rightarrow F2. The observed NHHS Fe^{II} doublet arose from some combination of modeling components F2, FC, and FM; the three cannot be distinguished by MB. Although this doublet represented just 9% of the intensity of the AFM0-40 spectrum, the absolute cellular concentration of the Fe^{II} species giving rise to it was significant. A

similar doublet has been observed along with the dominating nanoparticle doublet in Yah1-and Atm1-deficient mitochondria (33). The Fe^{II} doublet remained throughout the titration. Most of the NHHS Fe^{II} intensity probably arose from vacuolar Fe^{II} (F2 in the model), but this iron might have also been exported from vacuoles forming cytosolic Fe^{II} (FC in the model).

When [EST] was reduced to 10 nM in an AFM sample, the resulting spectrum (Fig. 3E) remained dominated by the NHHS Fe^{II} doublet. However, the low-energy line of this doublet broadened suggesting the development of nanoparticles MP. This feature increased in the 5 nM and 2.4 nM samples (Fig. 3, F and G). When [EST] = 0, in cells grown with 40 µM ⁵⁷Fe^{III} citrate, the overall spectral intensity (Fig. 3H) increased dramatically (more so when MM rather than CSM was used as the growth medium). Virtually all the extra spectral intensity arose from a quadrupole doublet attributed to nanoparticles.

Seguin *et al.* 2010 (6) reported that mutant aerobic cells accumulated large amounts of iron when [EST] = 0 but not when [EST] = 2.5 nM (at that concentration there was modest rise in cellular iron concentration relative to in WT cells). They also reported that aconitase activity was undetectable at [EST] = 0 but at WT levels when [EST] = 2.5 nM. Their results indicate a causal correlation between: a) loss of ISC activity; b) increased rate of iron import into the mitochondria; and c) increased level of mitochondrial nanoparticles.

[Insert Fig. 4]

We also examined the EPR spectra of mutant cells with different Yfh1 expression levels. AFM0-10 cells exhibited an intense broad EPR signal near g = 2.0 due to nanoparticles (Fig. 4, Panel A, dashed line). Similar signals have been observed in spectra of Yah1- and Atm1-depleted cells (31,33). In contrast, AFM2000-10 cells did not exhibit this signal (Fig. 4, Panel A, solid line), but they did exhibit an EPR signal at g = 4.3 undoubtedly due to vacuolar S = 5/2 Fe^{III} ions - similar to the g = 4.3 signal

exhibited by WT cells (14). We conclude from the EPR spectra that the concentration of vacuolar Fe^{III} in Yfh1-deficient cells was low. This agreed with the corresponding low-temperature MB spectra (e.g. Fig. 3D) which were largely (but perhaps not entirely) devoid of the magnetic feature due to vacuolar Fe^{III}.

AFM2000-10 cells exhibited the g = 4.3 EPR signal but not the broad g = 2 nanoparticle signal (Fig. 4B red spectrum). By comparing this to the dashed line spectrum of the top panel, we concluded that the decline in vacuolar Fe^{III} occurred at a higher Yfh1 concentration than that needed to generate nanoparticles. The decline of vacuolar Fe^{III} and formation of NHHS Fe^{II} were early titration events in the development of the Yfh1deficient phenotype. The oxidation of NHHS $Fe^{II} \rightarrow Fe^{III}$ ions and the aggregation of these Fe^{III} ions into nanoparticles were later titration events. This implied that the mechanism controlling vacuolar iron content, including redox state but perhaps also the rate of iron import into and export out of vacuoles, may not be regulated (or solely regulated) by ISCrelated processes occurring within mitochondria.

The EPR spectrum of HFM2000-10 cells (Fig. 4B, blue line) exhibited *neither* the g = 4.3 signal nor the broad g = 2 signal. This suggested that *hypoxic cells were devoid of both vacuolar Fe^{III} (F3) and nanoparticles (MP)*. MB spectra (see below) confirmed that and revealed that most iron in such cells was NHHS Fe^{II} (F2 + FC + FM combined). An O₂-dependence for oxidizing F2 \rightarrow F3 had not been previously recognized. Such an O₂-dependence is included in the model of Fig. 1.

Manganese species in Yfh1-Deficient cells: Although not the focus of this study, EPR spectra of mutant cells exhibited a noticeable hyperfine-split signal in the g=2 region due to mononuclear Mn^{II} ions. Its intensity was diminished in HFM2000-10 cells relative to AFM2000-10 cells (Fig. 4, Panel B red vs. blue

spectra). Under aerobic conditions, the parent strain contained $20 \pm 5 \mu M Mn (n = 2)$ which is similar to the average of previous reports for aerobic WT fermenting cells (18,19,42), namely $26 \pm 7 \mu M$. AFM0-40 cells contained substantially higher Mn concentrations (70 ± 11 μ M; n = 4) which may be related to an increased expression of Mn superoxide dismutase (MnSOD) in response to oxidative stress (43). Consistent with this, the cellular Mn concentration in our titration series increased 2-5 fold as the [EST] concentration decreased (data not shown). HFM0 cells contained $27 \pm 5 \mu M Mn (n = 2)$ which may reflect a return of MnSOD to WT levels under hypoxic conditions (44).

Nanoparticle loading declined in aerobic Yfh1-Deficient cells grown at high [IRON]: WT cells grown on media containing 40 µM 57Fe III citrate store high-spin Fe^{III} polyphosphate complexes in vacuoles (45); these ions exhibit magnetic MB features that spans from -10 to +10 mm/s velocity (Fig. 5B). WT cells grown with 1 µM ⁵⁷Fe^{III} citrate did not contain much vacuolar Fe^{III} (Fig. 5A); this is the standard state for WT yeast cells (18). Rather, these WT cells exhibited an intense NHHS Fe^{II} doublet for cells grown on [IRON] = 1 uM. Based on our model, this doublet arose from the sum of [FC] + [F2] + [FM] (caused by activation of the Iron-Regulon). We are not sure which of these species dominates, but it is probably [FC] or [F2]. Holmes-Hampton et al. observed similar behavior under iron-deficient conditions and attributed the strong NHHS Fe^{II} doublet mainly to F2 (18).

[Insert Fig. 5]

Under the same low-iron conditions, mutant Yfh1-deficient cells exhibited a fundamentally different MB spectrum, one dominated by nanoparticles. Essentially identical spectra were observed for AFM0-1 (Fig. 5C) or AFM0-10 (Fig. 5D) cells. Surprisingly, spectral intensity was independent of nutrient iron concentration within this range. This

differs from Auchere *et al.* (46) who reported that the extent of iron accumulation increases with increasing nutrient iron levels. However, comparisons are difficult because of differences in experimental details.

We were also surprised that spectra of Yfh1deficient mutant cells grown aerobically on 100 uM ⁵⁷Fe^{III} citrate were 5-fold *less* intense than those of cells grown in media containing lower iron concentrations (in Fig. 5, compare absorption [%] scale in E vs. in C or D). We observed a similar reduction in nanoparticle spectral intensity in three independent preparations. Curiously, this result implies that Yfh1-deficient cells grown on media containing high nutrient iron are less dysregulated than when grown on low nutrient iron. Consistent with this, Seguin et al. found that excess nutrient iron (up to 2.5 mM) improved the growth of Δ yfh1 cells (6).

AFM0 cells also lacked vacuolar Fe^{III} (Fig. 5, C-E) that is present in WT cells even at high iron (Fig. 5B). The AFM0 spectra also exhibited significant HS Fe^{II} features. Percentages of spectral features are listed in Table S2. Vacuolar iron export should accelerate in AFM cells for the same reason that these cells accumulate iron – i.e. activation of the Iron Regulon increases expression of both Fet3 and Fet5. However, the regulatory details may be more complicated.

[Insert Fig. 6]

Mössbauer of hypoxic (HFW and HFM) cells: We performed similar experiments on fermenting cells grown under hypoxic conditions. MB spectra of HFW cells were dominated by a NHHS Fe^{II} doublet (Fig. 6, A and B) and lacked features due to vacuolar Fe^{III}. ΔMtm1 and adenine-deficient WT cells exhibit similar spectra (38,47). The minor shoulder at ca. +1 mm/s in Fig. 6, A and B was likely the high-energy line of the CD.

Spectra of HFM0 cells were also dominated by a NHHS Fe^{II} doublet (Fig. 6, C and D). There was a small shoulder resolved from the

low-energy line of the main doublet which probably arose from the CD (Fig. 6C, arrow). The major difference, relative to WT cells, was that the spectral intensity for the NHHS Fe^{II} doublet was quite variable, with the intensity of some spectra comparable to WT spectra, while the intensity of other mutant spectra was greater than WT spectra (Fig. S1). We suspect that this variability was due to small differences in the percentage of O₂ used in growing hypoxic mutant cells.

Spectra of HFW-1, HFW-40, HFM0-1, and HFM0-40 cells did not exhibit the magnetic feature due to vacuolar Fe^{III} . With low $[O_2]$ bubbling through the growth medium, the rate of $F2 \rightarrow F3$ oxidation appears to have been slowed. A sensitive balance of factors, including $[O_2]$ levels, appears to control the oxidation state of vacuolar iron and the rate of iron import into the cell.

Mössbauer spectra of respiring cells: Although respiration requires O₂, the hypoxic conditions used here (~5% O₂) allowed both WT and mutant cells to respire slowly on glycerol/ethanol while limiting ROS damage. Thus, we investigated the iron content of hypoxic respiring cells. Mössbauer spectra of aerobic respiring ARW-40 cells (Fig. 7A) were comparable to those of fermenting AFW-40 cells (Fig. 3A or 5B) except that the CD contributed a higher spectral percentage, consistent with a greater use of mitochondria during respiration.

The spectrum of hypoxic HRW-40 cells (Fig. 7B) was dominated by the CD and a NHHS Fe^{II} doublet. The loss of vacuolar Fe^{III} (probably due to reduction to Fe^{II}) as respiring WT cells transitioned to hypoxic conditions indicated a sensitivity to metabolic mode. This suggested that the redox state of vacuolar iron in WT cells is determined by the O₂ status during cell growth (with lower O₂ favoring Fe^{II} vacuolar iron).

The spectrum of aerobic ARM0-40 mutant cells was dominated by nanoparticles, with

significant vacuolar Fe^{III} and little NHHS Fe^{II} (Fig. 7C). There is little doubt that the nanoparticles in both respiring and fermenting aerobic cells were in mitochondria; this accumulation indicated that the Iron Regulon under both metabolic modes was activated. Thus, aerobic mutant cells were strongly iron dysregulated, regardless of metabolic mode. However, respiring mutant cells must have been dysregulated differently than fermenting mutant cells because vacuolar Fe^{III} was present in respiring mutant cells but lacking in fermenting ones. Since both Fet3 and Fet5 are part of the Iron Regulon, both genes should have been strongly expressed in both the respiring and fermenting mutant cells. Our results suggest that Iron Regulon activation is not the only factor that determines the redox status of vacuolar iron.

Spectra of hypoxic respiring HRM0-40 cells exhibited a dominant vacuolar Fe^{III} signal, not a nanoparticle doublet (Fig. 7D). The NHHS Fe^{II} doublet was also intense. In contrast, the spectrum of hypoxic fermenting HFM0 cells were dominated by NHHS Fe^{II} (e.g. Fig. 6, C, D) with no NHHS Fe^{III} and little if any CD. The spectra of respiring hypoxic mutant cells overall were quite intense (compare to Fig. 3A), suggesting that the cells are dysregulated. In any event, these results suggest that the redox state of vacuolar iron and perhaps the rates of iron import/export into vacuoles are independent of the iron regulation/dysregulation the status mitochondria or whole cell.

[Insert Fig. 8]

Isolated Yfh1-deficient mitochondria from hypoxic cells: Mitochondria isolated from aerobic Yfh1-deficient fermenting cells accumulate large quantities of Fe^{III} oxyhydroxide nanoparticles (5). In contrast, mitochondria isolated from corresponding hypoxic cells in the current study were not ironoverloaded, regardless of whether mutant cells were grown with [IRON] = 1 or 40 (Fig. 8, C

and D). Rather the spectra were dominated by the CD, as in spectra of mitochondria from WT cells (18,48-50). Mitochondria from analogous HFW cells exhibited similar spectra (Fig. 8, A and B). In all four spectra, 50% - 60% of the intensity was due to the CD. Much of the remaining intensity was due to a NHHS Fe^{II} doublet. Previously reported spectra of mitochondria isolated from Yah1-deficient and Atm1-deficient cells grown under anaerobic/hypoxic conditions were similar (31,33).

We also examined mitochondria isolated from HRM0-40 and HRW-40 cells. In these cases, the dominating feature in both spectra was the CD (Fig. 9, A and B), similar to spectra of mitochondria from aerobic respiring WT cells (48-50). The mitochondria from these hypoxic cells were not iron-overloaded and did not display spectral features due to nanoparticles.

[Insert Fig. 9]

Aconitase activities were determined in four other batches of mitochondria isolated from cells grown under hypoxic conditions, one each for HRW-1, HRW-40, HRM0-1, and HRM0-40. Activities were $1.14 \pm 0.01, 1.07 \pm 0.22, 2.5 \pm 0.37$, and 1.31 ± 0.06 units/mg protein, respectively (uncertainties are standard deviations from four measurements). We conclude that mitochondria from both WT and mutant cells, grown under hypoxic conditions, had significant and comparable ISC activities.

Taken collectively, these results provided unambiguous spectroscopic and enzymatic evidence that [Fe₄S₄] clusters can be assembled and are stable in cells **lacking** Yfh1 - but only if hypoxic conditions are used.

Thus, the lack of ISCs in AFM cells is not directly due to the lack of Yfh1. Such clusters are synthesized in the absence of Yfh1, but at a slower rate (17). As long as O₂ concentrations in the matrix are low, clusters can be assembled. Perhaps the persulfide formed on Nfs1 is more stable under hypoxic conditions. Under aerobic conditions, perhaps more O₂

enters the mitochondrial matrix of mutant cells (due to a weakened Respiratory Shield) where it inhibits ISC assembly. O₂ also likely reacts with the Fe^{II} pool in the mitochondria. Both effects would weaken the shield in a vicious cycle.

Although the spectral features exhibited by mitochondria isolated from hypoxic respiring mutant (Fig. 9A) and WT (Fig. 9B) cells were qualitatively similar, the percent-effects differed significantly; the WT spectrum was more intense than the mutant spectrum (22% vs. 14%). Additionally, the MB cup for the WT sample was only ½ filled, whereas that for the mutant cells was ¾ filled. Taking these differences into account indicates that respiring mitochondria isolated from hypoxic WT cells contained nearly 5× as much iron as comparable mutant mitochondria (assuming the same purity).

Mathematical Model: We began with the ODE-based model used to simulate the $\Delta\Delta$ Mrs3/4 phenotype (19,36) and minimally modified it as necessary to simulate the Δ Yfh1 phenotype. The chemical model shown in Fig. 1 included 10 reactions (Table S3) and 9 components (defined in the *Introduction*). At the core of the model was the Respiratory Shield which can simulate an abrupt disease \rightleftharpoons healthy transition. The assumed rate-law expressions for all reactions of the model are in Table S3. These expressions, along with the reaction network, were used to generate a set of ODEs describing the change in component concentrations with time (Table S4).

In silico WT cells and hypoxic Δ Yfh cells were defined to grow at exponential rate $\alpha = 0.20 \, \text{hr}^{-1}$ whereas aerobic Δ Yfh cells grew more slowly. Cell growth was simulated by adding the term $-\alpha[C_i]$ to the ODE for each component C_i . This term allowed the system to be solved under an "expanding steady-state" condition (51) in which the volume of a cell is presumed to increase at a constant rate and the rates of all of the modelled reactions are time-invariant.

This was done by integrating the ODEs, along with a set of initial conditions, using the NDSolve function in *Mathematica 10* (Wolfram Software) at long integration times. *In silico* cells grew on fixed nutrients [IRON] = 1, 2, 11, or 41 μ M, and [RO2] = 5 (hypoxic) or 100 (aerobic) μ M. To account for the effects of hypoxia, O₂ was assumed to inhibit the reaction FM \rightarrow FS and to control the rate of vacuolar iron oxidation, R_{23} . As before, R_{mp} , R_{res} and R_{O2} had O₂ dependences included in their rate-law expressions.

The major modification relative to our previous model was to include Reg functions which allowed the system to be regulated. Previously, rates of regulated reactions were manually adjusted depending on cellular state. Here, they were augmented with Reg functions (35). Reg functions are surrogates of complex signal-transduction regulatory mechanisms, characterized by: a) the sensed species S (a component of the model); b) a set-point concentration of S ([S]_{sp}); and c) sensitivity factor n.

We initially attempted "global" regulation by assuming Reg±(FS) functions for reactions R_{cyt} , R_{isu} , R_{vac} , and R_{23} . Doing so implied control by the Aft1/2-dependent Iron Regulon, the most well-established mechanism of iron regulation in yeast cells. However, this attempt proved incapable of simulating observed behavior. A Reg-(FS) function successfully regulated R_{cyt} , but the same function regulating Rmit afforded excessively high [FM] and low [FS]. This mismatch was corrected by regulating R_{mit} with a Reg-(FM) function. R_{vac} and R_{23} were best regulated by assuming the "dual" function $\{Reg+(FS)\cdot Reg+(FC)\}$ in which both high [FS] and [FC] contributed to increasing the flow of iron into vacuoles. We also added a Reg-(O2) function to regulate R_{isu} .

We focused on 5 different cellular states, including aerobic WT, hypoxic WT, aerobic $\Delta Y fh1$, hypoxic $\Delta Y fh1$, and aerobic $\Delta \Delta Mrs 3/4$. The model included 35 adjustable parameters (Table S5). For these parameters, we initially

assumed previous values (36), and adjusted them conservatively to achieve desired behavior. Value of 14 parameters remained invariant (36). Values for 14 other parameters were changed relative to our previous study but were invariant for all 5 current cellular states.

The sensitivity of the WT aerobic model to variations in parameters revealed that 4 of the 9 most sensitive parameters involved the ISU reaction in mitochondria and 3 involved iron import into the cell (Table S8). Of the 6 least sensitive parameters, 4 involved vacuoles.

We assessed the viability of simulations qualitatively by their ability to mimic certain phenotypic behaviors while adhering to experimental iron concentrations. This approach was effective in generating the desired *qualitative* behavior. However, we cannot guarantee that the parameters in Table S5 are unique in eliciting these behaviors or are the globally best at doing so.

We first optimized the behavior of WT and $\Delta\Delta Mrs3/4$ simulations and then focused on WT hypoxic, $\Delta Y fh$ aerobic, and $\Delta Y fh$ hypoxic states. To simulate these latter states, we adjusted the easily-justifiable parameters first and then minimally adjusted remaining parameters as needed. Of the remaining 7 adjustable parameters, 4 were easily justified according to the established properties of the particular cellular state. Specifically, R_{O2} was lowered to create hypoxic conditions, R_{isu} was lowered to create Yfh1-deficient conditions, as expected for Yfh1-deficient conditions, and R_{mit} was lowered to slow mitochondrial iron import in $\Delta\Delta Mrs 3/4$ cells, again as expected for Mrs3/4-deficient conditions. The growth rate (α) for aerobic Δ Yfh1 cells was set lower than for WT cells, hypoxic ΔYfh1 cells, and ΔΔMrs3/4 cells grown at high nutrient iron, consistent with observations. This left only 3 parameters that were adjusted without clear justification. Of those, K_{α} (Michaelis-Mentenlike parameter describing growth rate) was adjusted for only 1 of 5 states, and K_N (same for iron import into the cell) and $k_{cia-max}$ (rateconstant for generating CIA) were adjusted for only 2 of 5 states. The optimized model simulated the phenotype of these 5 cellular states with overall semi-quantitative fidelity (Table S6).

[Insert Fig. 10]

In Fig. 10, simulations were compared to MB spectra. Contributions from [FC], [FM], and [F2] were summed and normalized to simulated cellular iron concentrations (Table S7), as this allowed comparison to the NHHS Fe^{II} species observed by MB spectroscopy. Likewise, [FS] and [CIA] simulations were summed and normalized in the same way, so that they could be compared to the central quadrupole doublet (CD) observed by MB. Similarly, [MP] and [VP] were summed and normalized, so that they could be compared to the nanoparticle contribution observed in MB spectra. Finally, [F3] was normalized and compared to the NHHS Fe^{III} feature in MB spectra.

For aerobic WT cells, simulations correctly predicted that vacuolar Fe^{III} would dominate MB spectra of these cells at high [IRON]. They also correctly predicted similar relative intensities of the CD, NHHS Fe^{II}, and nanoparticles, in that order (Fig. 10A). As [IRON] declined, simulated vacuolar Fe^{III} levels declined causing the CD to increase percentagewise, as observed in Fig. 5, A and B. Simulated Fe^{III} and nanoparticle percentages were low, as observed.

For hypoxic WT cells, simulations at high [IRON] were dominated by Fe^{II}, as observed (compare Fig. 10B to Fig. 6, A and B). This was followed by the CD, and little Fe^{III} or nanoparticle intensities. Simulations indicated more CD (relative to Fe^{II}) than was observed.

For aerobic mutant cells, nanoparticles dominated as observed (compare Fig. 10C to Fig. 5, C, D, and E), and they declined somewhat at high [IRON], also as observed. For hypoxic mutant cells, simulated Fe^{II} dominated as observed (compare Fig. 10D to

Fig. 6 C, and D). Relative to WT cells, the CD was lower, also as observed.

[Insert Fig. 11]

The simulations shown in Fig. 11, Panel A should be compared to the titration of Fig. 3; both show the effects of lowering the expression level of Yfh1. The right-side of the Fig. 11, top panel plot represents aerobic WT conditions while the left-side represents aerobic Yfh1-deficient conditions ([EST] = 0). Simulations showed an immediate drop in the CD followed by a decline of Fe^{III}. In actual titrations, Fe^{III} declined *before* the CD. In the simulated titration, as Yfh1 levels declined, Fe^{II} increased followed by nanoparticles.

The other panels of Fig. 11 are plots showing the effect of decreasing oxygen levels on WT and mutant cells. For both strains, simulated [O2] concentrations declined as the oxygen concentration in the growth medium (RO2) declined. For WT cells, this occurs with a shift from Fe^{III} to Fe^{II} (as observed) while the concentration of the CD remained constant at ~ 30%. In real spectra, the CD contribution is less intense. For simulations of mutant cells, nanoparticles dominated, as observed. As [O2] levels declined, simulations showed that nanoparticles declined as Fe^{II} increased (as observed). Simulated [FS] was low, whereas in reality, the CD in mitochondria isolated from hypoxic cells had an intensity comparable to in WT mitochondria (See Fig. 8 and 9). Encouragingly, simulated [FS] did increase as in-silico cells approached hypoxia. ΔΔMrs3/4 simulations still showed the recovery of mitochondrial iron distribution with increasing nutrient iron, and a large amount of vacuolar Fe^{III} with respect to WT (Fig. S2).

Given the complexity of the model and the different phenotypes observed for the 5 states, the simulations overall were qualitatively consistent. They provide significant support for the mechanism of Fig. 1 and the major assumptions made in its development.

Discussion

Disentangling the Yfh1 phenotype in yeast is notoriously difficult; it has been the topic of > 400 research articles since it was first described in 1997 (52). We used the results of this study, primarily obtained from Mössbauer spectra, along with published results from the literature, to develop a chemical/mathematical model (Fig. 1) that can explain this phenotype on the molecular level and in semi-quantitative terms. Apart from our related earlier math models (35,36), no comparable models have been published. Although not perfect, our model represents the best current mechanistic understanding of how healthy yeast cells transition to the diseased state associated with Friedreich's Ataxia.

Changes during Yfh1-titration reveal the cell's response to Yfh1-deficiency. In the titration reported here, the earliest MBobservable event as Yfh1 expression in AFM cells declined from WT levels was the reduction of vacuolar Fe^{III} to Fe^{II}. This reduction occurred prior to the accumulation of iron in the cell or mitochondria, and prior to the loss of [Fe₄S₄]²⁺ clusters and LS Fe^{II} hemes (as reflected in the CD), much of which is in mitochondria. We were unable to determine whether F2 remained in the vacuole or moved into the cytosol. Nor could we determine whether the observed spectral changes arose from changes in the genetic expression of the iron transporters on the vacuolar membrane or from epigenetic effects e.g. changes in the concentrations of a metabolite that affected the rate of reduction or transport (e.g. NADPH). In any event, these results reveal an independence between the iron status of vacuoles and the activity of Yfh1 in mitochondria; amazingly, vacuolar iron is more sensitive to modest in expression declines Yfh1than mitochondrial iron (even though Yfh1 is a mitochondrial protein). One speculative possibility is that the redox properties of the vacuoles are connected to the activity of mitochondria through metabolites such as

NAD(P)H. For example, reduced consumption of NADH due to impaired respiration might increase NADH which might be converted to NADPH by dedicated kinases thus promoting reduction of vacuolar Fe^{III}.

titration Later events included the accumulation of cellular iron and the loss of the CD. These two processes occurred synchronously, suggesting a tight mechanistic connection between the rate of cellular iron import (R_{cvt}) , mitochondrial iron import (R_{mit}) , ISC assembly (R_{isu}) and nanoparticle formation (R_{mp}) . R_{cvt} probably increased when the declining concentration of Yfh1 began to inhibit R_{isu} . The reduction in [FS] caused by this inhibition probably activated the Aft1/2dependent Iron Regulon causing R_{cyt} to increase. From these results alone, one might conclude that the same regulatory mechanism controls R_{mit} but the rate of mitochondrial iron import may be regulated differently. Our model assumes that R_{mp} is controlled by O₂ levels in mitochondria and is not genetically regulated.

Seguin et al. estimated that the Yfh1 threshold for activating the Iron Regulon is ~ 7% of WT levels (6). Below this, aconitase activity drops precipitously. At [EST] = 2.5 nM, aconitase activity was similar to WT activity, whereas at [EST] = 0 nM, activity was zero. We observed similar near disproportionate behavior in terms of iron accumulation and nanoparticle formation, in that both developed abruptly with a small change in [EST]. The Respiratory Shield aspect of the Fig. 1 model allows such abrupt behavior due to its vicious-cycle nature.

In 2010, Moreno-Cermeno et al. examined a strain of yeast in which Yfh1 could be depleted over time by adding doxycycline to the growth medium (53). Iron accumulated soon after Yfh1 started to deplete. This was followed by a decline in respiration, and then a decline of ISC enzyme activities. They concluded that the Iron Regulon activates and cellular iron accumulates *before* ISC activity declines suggesting that Yfh1 is *not* primarily involved

in either ISC or heme biosynthesis. In contrast, our results suggest that Yfh1 primarily accelerates the rate of ISC/heme assembly and that the other events associated with a Yfh1 deficiency arise secondarily because of a decline in ISC/heme assembly rates.

Iron homeostasis partially recovers in Yfh1deficient cells grown on high nutrient iron: Unexpectedly, AFM0-100 cells accumulated less iron as nanoparticles than similar cells grown with lower Fe^{III} citrate supplementation. The mitochondrial membrane potential in Yfh1-deficient cells was 20-fold lower than in WT cells, but it could be partially restored by growing Yfh1-deficient cells in media containing high levels of iron (32).Accordingly, we suggest a connection between membrane potential, R_{mit} , and R_{mp} . The Respiratory Shield hypothesis implies such a connection since respiration establishes a proton gradient and hence a membrane potential. We hypothesize that Yfh1-deficient mitochondria in aerobically grown cells synthesize ISCs at a rate that is limited by [FM], and that [FM] is influenced by [FC] (via rate R_{mit}). We further hypothesize that ISCs are not observed by MB spectroscopy or evidenced by aconitase activity because the high levels of O₂ in mitochondria under these conditions inhibit the FM \rightarrow FS reaction. When aerobic cells are grown in high-iron media, the rate of assembly increases because increases (due to increased [FC]). This fortifies the Respiratory Shield in ΔΔMrs3/4 cells grown under iron-replete conditions (36). The observed recovery at high nutrient iron would be difficult to explain without the Respiratory Shield concept.

Hypoxic growth reveals that Yfh1 is not required for ISC assembly: The dominance of the CD in MB spectra of mitochondria isolated from HFM0 and HRM0 cells was typical of WT mitochondria, regardless of whether mutant cells were grown with [IRON] = 1 or

40. This indicates that *Yfh1* is not required for *ISC synthesis*. We cannot distinguish whether ISCs in aerobic Yfh1-deficient cells are synthesized and then degraded by O_2 , or not synthesized at all (due to inhibition by O_2). Previous results suggest the latter (32,54), and so we assumed that O_2 inhibits the FM \rightarrow FS reaction. Doing so also strengthens the viciouscycle nature of the Respiratory Shield.

Yfh1-deficient cells can generate ISCs and hemes when grown under anaerobic/hypoxic conditions (17,30,32), and our results support this. ΔYfh1 cells display no growth defects when cultured anaerobically and ISCs can be assembled (as evidenced from by aconitase activities), though probably at lower rate than for WT cells. These mutant cells have increased levels of oxidative damage when grown aerobically.

ISC synthesis in Yfh1-deficient cells may be more O₂ sensitive than WT cells. Yfh1 forms an ISC assembly complex with Nfs1, Isd11, Acp1, and Isu1/2. In that complex, Yfh1 may guide the persulfide on the Nfs1 flexible loop to its destination on a recipient cysteine residue of Isu1/2. The Nfs1 persulfide and the cysteine recipient may be particularly O₂ sensitive, leading to a greater requirement for Yfh1 in air versus hypoxic conditions.

Mootha and coworkers recently confirmed the effect of hypoxia on yfh1-deficient yeast and extended such studies to frataxin-deficient human cells, nematode worms, and mice (54). They reported that frataxin was not required to achieve WT levels of ISC assembly activity under hypoxic conditions. They also found that hypoxia boosts ISC biosynthetic activity rather than suppresses ISC degradation, confirming earlier studies. However, they did not cite any of the earlier pioneering studies on the effects of hypoxia in Yfh1-deficient yeast cells (17,30,32).

The effect of hypoxia (and thus O₂) on Yfh1-deficient cells helps disentangle how iron homeostasis is regulated. Our studies show that **both** O₂ and a deficiency of Yfh1 are required

for yeast cells to be iron-dysregulated and exhibit the classic phenotype involving loss of ISC activity, accumulation of Fe^{III} oxyhydroxide nanoparticles in mitochondria, increase in ROS, decline of respiratory ability etc. The model of Fig. 1 describes the interplay between these two factors in mechanistic terms, with the Respiratory Shield playing an essential role.

Effect of hypoxia in Yfh1-deficient cells is specific to Yfh1-deficiency. The hypoxic/anaerobic phenotypes cells of deficient in Atm1 or Yah1 are similar to that of Yfh1-deficient cells. As with Yfh1-deficient cells, the iron content of mitochondria isolated from aerobic fermenting Atm1-deficient and Yah1-deficient cells is an order-of-magnitude higher than WT mitochondria (31,33). Atm1deficent mitochondria from aerobically grown cells are massively overloaded nanoparticles and do not exhibit an ISC doublet in their MB spectra. Their aconitase activities are near zero and vacuolar Fe^{III} is absent. Thus, iron is dysregulated in aerobic Atm1-deficient cells. The best-studied mechanism of iron homeostasis is thought to involve Atm1 exporting "X-S" which connects the ISC activity of mitochondria with the Aft1/2dependent Iron Regulon that controls iron import into the cell and mitochondria. Accordingly, the lack of X-S caused by an Atm1 deficiency upregulates the import of Fe into the cell and mitochondria. Yahl-deficient cells grown aerobically show a similar phenotype indicating iron dysregulation.

However, mitochondria isolated from Atml-and Yahl-deficient mutant cells grown under anaerobic/hypoxic conditions are **not** overloaded with nanoparticles. Hypoxic Atml-deficient cells contain cytochromes at WT levels and have significant aconitase activities. Like Yfhl, Atml is *not* required for mitochondrial ISC cluster assembly or heme biosynthesis – and such clusters are observed *if cells are grown under anaerobic/hypoxic*

conditions. Unlike Atm1 and Yfh1, Yah1 appears to be essential for ISC assembly, since the MB spectrum of isolated mitochondria from these cells, when grown hypoxically, do not exhibit a distinct CD as is observed in mitochondria isolated from hypoxic Atm1- or yfh1-deficient cells.

The results of Miao et al. for mitochondria isolated from Atm1-deficient cells grown under anaerobic conditions (33) cannot be easily explained by assuming that Atm1 exports X-S in the mechanism of Aft1/2dependent iron regulation (55). (Atm1 likely exports X-S for use in cytosolic ISC assembly.). The contents and distribution of Fe in mitochondria isolated from anaerobic WT and Atm1-depleted cells are quite similar suggesting that the homeostatic mechanism regulating mitochondrial iron operational even in the absence of Atm1, as long as O2 is excluded or is present at low concentrations. This suggestion needs to be evaluated further.

The effect of hypoxia in rescuing the nanoparticle accumulation phenotype does not appear specific to a specific protein deficiency. Rather, the curative effect of hypoxia seems to be a general response to a deficiency in various proteins which, we suggest, collectively contribute to a major mitochondrial process such as respiration. The Respiratory Shield again comes to mind because its function to slow O₂ from diffusing into the mitochondrial matrix depends on the concerted functioning of many proteins. Defects in any of these proteins could weaken the shield, leading to a massive accumulation of nanoparticles under aerobic conditions. The same defects would be present under anaerobic conditions but in that case a weakened shield might be sufficient to prevent nanoparticle formation and dysregulation when coupled with the lower oxygen levels associated with hypoxic/anaerobic conditions.

If the rate of cellular iron import (R_{cyt}) were regulated the same as the rate of mitochondrial iron import (R_{mit}), a change in one rate would

always be matched by a similar change in the other. Such matching occurs for yfh1-deficient cells under aerobic conditions (both rates increase), and it may occur under hypoxic conditions (both rates do not increase).

Other evidence suggests the opposite. The "triple mutant" strain in which Yfh1, Mrs3, and Mrs4 have all been deleted ($\Delta\Delta\Delta$) exhibits behavior suggesting independent regulation of R_{cyt} and R_{mit} . The iron that accumulates as nanoparticles in Yfh1-deficient mitochondria is imported via Mrs3/4 transporters on the inner mitochondrial membrane. The $\Delta\Delta\Delta$ mutant does not accumulate iron in mitochondria but does accumulate iron in the cell (17). This suggests that $\Delta\Delta\Delta$ cells are iron-dysregulated (probably due to low [FS]) even though their mitochondria are not, implying independent regulation between cellular iron import and mitochondrial iron import. Under hypoxic conditions, the $\Delta\Delta\Delta$ strain grows slowly in unsupplemented media, but faster in high-iron media as more iron enters the mitochondria through low-affinity importers such as Rim2 (56). This behavior is reminiscent of the ΔΔMrs3/4 double-deletion strain in which the Respiratory Shield was strengthened by an increased Rmit under iron-replete conditions (19).

In our current model, we presumed that R_{cvt} is regulated by mitochondrial ISC production (i.e. by [FS]) while R_{mit} is regulated by [FM]. This allowed us to explain why mitochondria import massive amounts of iron in Yfh1-, Atm-, Yah1mutant cells under aerobic but not hypoxic conditions. Under aerobic conditions, both [FS] and [FM] are low and [MP] is high (the mitochondria are filled with nanoparticles), such that R_{cyt} and R_{mit} are both activated. [FS] is low because the lack of Yfh1 slows the reaction FM \rightarrow FS; [FM] is low because the Respiratory Shield is weakened (due to low [FS]) and the increased O₂ that diffuses into the mitochondria reacts quickly with FM to generate MP. Under hypoxic conditions, the shield weakens, but is sufficiently strong to

slow the rate of O_2 diffusion into the matrix (since external $[O_2]$ is low). This prevents [FM] from declining (converting to MP) such that R_{mit} is not activated.

Redox state of vacuolar iron depends on O₂ levels in WT cells but on metabolic state in mutant cells. Under both aerobic and hypoxic growth conditions, current and previous studies suggest that mitochondria from fermenting or respiring WT cells are similar in terms of MB spectra (dominated by the CD with some NHHS Fe^{II}). Under aerobic conditions, vacuolar iron is Fe^{III} while under hypoxic conditions, vacuolar iron in WT cells is Fe^{II} (perhaps mobilized from vacuoles to cytosol). This implies an independence between vacuolar and mitochondrial iron.

The corresponding situation was different for the mutant; here, under both aerobic and hypoxic growth, vacuolar iron remained Fe^{III} when cells respired but was reduced to Fe^{II} when cells fermented. Mutant mitochondria under hypoxic conditions were qualitatively indistinguishable from WT mitochondria whereas mutant mitochondria under aerobic conditions were almost certainly overloaded with nanoparticles (we did not isolate mitochondria under this condition in this study but whole-cell Mössbauer showed an intense nanoparticle doublet indistinguishable from spectra of mitochondria previously isolated from Yfh1-deficient cells). This implies that redox state (and perhaps mobilization) of vacuolar iron is controlled independently of the regulatory process that controls mitochondrial iron.

The proposed regulatory independence of vacuolar vs. mitochondrial iron is also evident in aerobic WT cells grown under [IRON] = 1 vs. 40. Under both nutrient conditions, the growth rate of cells is essentially invariant and mitochondria from both cells are "normal". By contrast, vacuoles are largely devoid of iron when cells are grown in 1 μ M Fe and largely filled when grown in 40 μ M Fe. This implies

that filling vacuoles (due to R_{vac} in the model) is regulated by something besides or in addition to [FS] activity in mitochondria. In the model, R_{vac} was regulated by both [FC] and [FS]. This dual regulation can also explain why vacuoles are devoid of iron in Yfh1-deficient cells grown under aerobic conditions, in that the increased flow of FC into mitochondria (due to the decline of [FM]) results in low [FC], which then promotes the exodus (or inhibits the import) of iron from/to vacuoles.

Synchronized vs. independent Iron Regulation: Our results and modeling provide some evidence for regulatory independence among the major sites of regulation in the trafficking of iron in yeast cells; these include the site of cellular iron import, mitochondrial iron import, vacuolar iron import/export, and vacuolar redox state.

The extreme possibilities for regulating multiple sites of iron trafficking in cells are global synchronization, regulated by a common sensed species, or complete independence, achieved by separate regulatory processes operating locally on different reactions. A spectrum of intermediate situations in which there is some degree of independence and some degree of synchronization is also possible. On a molecular level, independence can arise from variations in the strength or kinetics of binding of the same transcription factor to promotor sites of the regulated genes. It may arise from the involvement of multiple transcription factors in controlling regulation. Transcription factors Aft1, Aft2, Yap5, and Cth2 are all involved in iron regulation, but are only partially understood at the cellular or systems level. Perhaps these and other unknown factors are responsible for the degree of regulatory independence that we observed.

Advantages of mathematical modeling: Understanding the development of the frataxindeficient phenotype requires quantitative mathematical models to integrate myriad interrelated events. Our model represents a quantitative hypothesis regarding the mechanism of iron trafficking and regulation in a yeast cell. Some experiments reported here were used to test the model and determine whether it has predictive power. The model of Fig. 1 evolved from earlier textual statements (30), as well as pictorial (6,31,33) and mathematical models (35,36).

Extending this approach to iron metabolism in human cells is a long-term objective. Such a model, with sufficient complexity and realism, may help develop new therapies and better treatments of Friedreich's ataxia.

Conclusions:

The major conclusions of this study are:

- The first event to occur as Yfh1 levels decline is a reduction of vacuolar Fe^{III} and an increase in NHHS Fe^{II}. Following this is a decline of ISCs and rise of mitochondrial nanoparticles.
- Both hypoxic WT and Yfh1-deficient cells lack vacuolar Fe^{III} and nanoparticles; they are dominated by NHHS Fe^{II} followed by ISCs.
- Aerobic Yfh1-deficient cells contained higher Mn concentrations than WT cells.
- Most iron in aerobic Yfh1-deficient cells is nanoparticles. Mutant cells grown on higher nutrient iron contained fewer nanoparticles.
- Hypoxic Yfh1-deficient cells are not iron dysregulated.
- The redox state of vacuolar iron is sensitive to the O₂ level during cell growth.
- The redox state of vacuolar iron and perhaps the rates of vacuolar iron import/export are independent of the iron regulation/dysfunction status of the mitochondria or whole cells.
- Mitochondria from Yfh1-deficient cells grown hypoxically do not accumulate nanoparticles but contain

- ISCs. Yfh1 stimulates ISC assembly but is NOT essential for it.
- A developed mathematical model of the kinetics of iron trafficking and regulation in growing yeast cells could explain semi-quantitatively the behavior of 5 different cellular states.
- According to the model, under healthy conditions, respiration slows the diffusion of O₂ into the matrix. Yfh1 deficiency slows the rate of ISC assembly, allowing more O₂ to enter the matrix and reacts with the Fe^{II} pool to generate nanoparticles. O₂ also inhibits ISC assembly, creating a vicious cycle that culminates in the diseased state.
- Assuming that global cellular regulation is controlled by the ISC activity in the mitochondria was less able to reproduce observed behavior than assuming local independent regulation.

Experimental Procedures

Yeast strains and cell growth: ERyfh1 cells were constructed from the YPH499 parent strain by promoter swap in which the YFH1 open reading frame was placed under control of the GAL1 promoter. The plasmid pGEV4-LEU2 was inserted and GAL4 was deleted, thereby creating a strain in which the YFH1 open reading frame was placed under control of an estradiol regulated promoter (MATa ura3-52, lys2-801 (amber) ade2-101 (ochre) trp1-Δ63 leu2-Δ1 cyh2 Δgal4::KanMX6 HIS3MX6pGAL1-YFH1[pGEV-LEU2] (6,41,57). Cells were maintained on minimal medium agar plates without leucine to select for the pGEV plasmid and with 5 µM estradiol to maintain Yfh1 expression. For some batches, cells were inoculated into liquid minimal media lacking leucine but containing estradiol at various concentrations. For other batches, CSM (Sunrise Science) medium lacking leucine was used. For hypoxic growths, 50 mL of aerobically grown cultures were used to inoculate larger cultures that had been supplemented with ergosterol (20 mg/L), tween-80 (1 mL/L), and antifoam B (Sigma Aldrich, 100 ppm final concentration) (31,33). Cultures were vigorously bubbled with a 95:5 N₂:O₂ or 3:1 N₂:air gas mixture to render them hypoxic. Whole cell cultures were harvested by centrifugation at $5000 \times g$ for 5 min. Cells were washed $3\times$ in a solution of $100 \mu M$ EDTA, and then $3\times$ in distilled, deionized water. Cells were packed into either a Mössbauer cup or EPR tube by centrifugation and frozen in LN₂.

Mössbauer and EPR spectroscopies: MB spectra were collected on a MS4 WRC spectrometer (SEE Co, Edina MN) at 5–6 K and 0.05 T. The magnetic field was applied parallel to the gamma radiation. An α -iron foil was used for RT calibration. X-band EPR spectra were collected using a Bruker Elexsis E500 spectrometer.

Mitochondria *Isolations:* Cells were harvested during exponential phase from a custom-built 24 L glass/titanium bioreactor. For hypoxic growths, two bioreactors were grown in parallel. Upon harvesting, liquid culture was pumped into a refrigerated anaerobic glove box for collection into centrifuge bottles. Filled bottles were removed from the box, centrifuged, and returned to the where pellets were combined. box Mitochondria were purified anaerobically from pellets as described (19). Organelles were frozen in MB cups, EPR tubes, or Eppendorf tubes for later analysis.

Metal Analysis and Aconitase Assays: Metal analyses were performed as described (58) using 5% trace-metal-grade nitric acid; 2.5% H₂O₂ were added to samples as needed. Aconitase assays were performed essentially as described (58). Isolated mitochondria were lysed and their protein contents were determined by the BCA assay. Approximately

16-32 μ g of mitochondrial protein in a lysis solution was added to reaction buffer containing 20 mM NaCl, 20 mM Tris-HCl, and 1 mM cis-aconitic acid (final concentrations). The decline in absorbance of the resulting solution at 240 nm was monitored for 6 min, and the slope was used to calculate activity (1 unit = 1 μ mol cis-aconitic acid/min).

Western Blot: The blot was done essentially as described (13). Crude mitochondria were isolated as above except without the ultracentrifugation step. The frataxin primary antibody was mixed in the TBST:milk solution at a concentration ratio of 1:100. The ratio for the porin antibody was 1:500. samples were incubated 1 hr at room temp and then overnight at 4 C. Secondary antibody was prepared at a concentration ratio of 1:500 for frataxin and 1:2500 for porin, then incubated 2 hr at RT and monitored by chemiluminescence (13).

Data Availability Statement: All data are contained within the manuscript and SI.

Acknowledgments: This work was supported by the National Science Foundation (MCB-1817389), the National Institutes of Health (GM127021 to PAL and GM107542 to AD), and the Robert A. Welch Foundation (A1170). The content is solely the responsibility of the authors and does not necessarily represent the views of the NIH, the NSF, or the Welch Foundation.

Conflict of interest: The authors declare that they have no conflicts of interest with the contents of this article.

FOOTNOTES

To whom corresponding should be addressed: Paul A. Lindahl, Department of Chemistry, Texas A&M University, College Station TX 77843-3255. Phone, 979-845-0956; Fax, 979-845-4719, email: Lindahl@chem.tamu.edu.

¹Texas A&M University, Department of Chemistry, College Station, TX 77843-3255 USA.

²Charleston Southern University, Department of Chemistry College of Science and Mathematics, Charleston SC 29406, USA.

³University of Pennsylvania, Department of Medicine, Division of Hematology-Oncology, Perelman School of Medicine. Philadelphia, PA 19104, USA.

⁴Texas A&M University, Department of Biochemistry and Biophysics, College Station, TX 77843 USA.

⁵Abbreviations used: α, exponential growth rate of cells: CD, central quadrupole doublet: CIA, cytosolic iron not associated with FC; ΔΔΔ, strain of yeast in which Yfh1, Mrs3, and Mrs4 have been deleted; EPR, electron paramagnetic resonance; EST, extradiol; F2, vacuolar Fe^{II}; F3, vacuolar Fe^{III}; FC, cytosolic iron; FM, mitochondrial Fe^{II} pool; FS, ironsulfur clusters and Fe^{II} hemes, many used in respiration; ISC, iron sulfur cluster; MB, Mössbauer; MP, mitochondrial nanoparticles; N, nutrient iron (Fe^{III} citrate); NHHS, nonheme high spin; ODE, ordinary differential equation; Reg±(S), regulatory functions exhibiting positive or negative feedback, sensing species S; ROS, reactive oxygen species; Yfh1, Yeast vacuolar frataxin homolog 1: VP. nanoparticles; WT, wild type.

REFERENCES

- 1. Cook A and Giunti P (2017) Friedreich's ataxia: clinical features, pathogenesis, and management. *Brit. Med. Bulletin* **124**, 19-30.
- 2. Tsai, C.-L. and Barondeau, D.P. (2010) Human Frataxin is an Allosteric Switch that Activates the Fe-S Cluster Biosynthetic Complex. *Biochemistry*, **49**, 9132-9139.

- 3. Pandey, A.; Gordon, DM.; Pain, J; Stemmler, TL.; Dancis, A; Pain, D (2013) Frataxin Directly Stimulates Mitochondrial Cysteine Desulfurase by Exposing Substrate-binding Sites, and a Mutant Fe-S Cluster Scaffold Protein with Frataxin-bypassing Ability Acts Similarly. *J. Biol. Chem.* **288**, 36773-36786.
- 4. Babcock M, deSilva D, Oaks R, Davis-Kaplan S, Jiralerspong S, Montermini L, et al. (1997) Regulation of mitochondrial iron accumulation by Yfh1p, a putative homolog of frataxin. *Science* **276**, 1709–1712.
- 5. Lesuisse E, Santos R, Matzanke BF, Knight SA, Camadro JM, Dancis A (2003) Iron use for haeme synthesis is under control of the yeast frataxin homologue (Yfh1). *Hum. Mol. Genet.* **12**, 879–889.
- 6. Seguin A, Sutak R, Bulteau A-L, Garcia-Serres R, Oddou J.L, Lefevre S., Santos R, Dancis A, Camadro JM, Latour JM, Lesuisse E. (2010) Evidence that yeast frataxin is not an iron storage protein in vivo. *Biochim. Biophys. Acta*, **1802**, 531-538.
- 7. Whitnall, M; Rahmanto, YS; Huang, M. L. H.; Saletta, F; Lok, HC; Gutierrez, L; Lazaro, FJ.; Fleming, AJ; St Pierre, TG. Mikhael, MR.; Ponka, P; Richardson, DR. (2012) Identification of non-ferritin mitochondrial iron deposits in a mouse model of Friedreich ataxia. *Proc. Natl Acad. Sci USA* **109**, 20590-20595.
- 8. Martelli A and Puccio H. (2014) Dysregulation of cellular iron metabolism in Friedreich ataxia: from primary iron-sulfur cluster deficit to mitochondrial iron accumulation. *Frontiers in Pharmacology* 5, Article 130. DOI: 10.3389/fphar.2014.00130

- 9. Foury, F. (1999) Low iron concentration and aconitase deficiency in a yeast frataxin homologue deficient strain. *FEBS Lett.* **456**, 281-284.
- 10. Karthikeyan, G., Lewis, L.K. (2002) The mitochondrial protein frataxin prevents nuclear damage. *Human Mol. Genetics* **11**, 1351-1362.
- 11. Hassett, RF; Romeo, AM; Kosman, DJ (1998) Regulation of high affinity iron uptake in the yeast *Saccharomyces cerevisiae* Role of dioxygen and Fe(II). *J. Biol. Chem.* **273**, 7628-7636.
- 12. Jensen, L.T. and Culotta, V.C. (2002) Regulation of *Saccharomyces cerevisiae* FET4 by oxygen and iron. *J. Mol. Biol.* **318**, 251-260.
- 13. Nguyen, T.Q., Kim, J.E., Brawley, H.N., Lindahl, P.A. (2020) Chromatographic detection of low-molecular-mass metal complexes in the cytosol of *Saccharomyces cerevisiae*. *Metallomics*, **12**, 1094-1105.
- 14. Li, L.T., Chen, O.S., Ward, D.M., Kaplan, J. (2001) CCC1 is a transporter that mediates vacuolar iron storage in yeast. *J. Biol. Chem.* **276**, 29515-29519.
- 15. Cockrell, A. L., Holmes-Hampton, G. P., McCormick, S. P., Chakrabarti, M., and Lindahl, P. A. (2011) Mössbauer and EPR study of iron in vacuoles from fermenting *Saccharomyces cerevisiae*. *Biochemistry* **50**, 10275–10283.
- 16. Mühlenhoff, U., Hoffmann, B., Richter, N., Rietzschel, N., Spantgar, F., Stehling, O., Uzarska, MA., Lill, R. (2015) Compartmentalization of iron between mitochondria and the cytosol and its regulation. *Eur. J. Cell Biol.* **94**, 292-308.
- 17. Zhang, Y., Lyver, E. R., Knight, S. A., Lesuisse, E., and Dancis, A. (2005) Frataxin

- and mitochondrial carrier proteins, Mrs3p and Mrs4p, cooperate in providing iron for heme synthesis. *J. Biol. Chem.* **280**, 19794–19807.
- 18. Holmes-Hampton, G. P., Jhurry, N. D., McCormick, S. P., and Lindahl, P. A. (2013) Iron content of *Saccharomyces cerevisiae* cells grown under iron-deficient and iron-overload conditions. *Biochemistry* **52**, 105–114.
- 19. Moore, MJ; Wofford, JD, Dancis, A., and Lindahl PA (2018) Recovery of Mrs3ΔMrs4Δ *Saccharomyces cerevisiae* cells under ironsufficient conditions and the role of Fe₅₈₀. *Biochemistry* 2018, **57**, 672–683.
- 20. Ramos-Alonso, L., Romero, A.M., Martinez-Pastor, M.T., Puig, S. (2020) Iron Regulatory Mechanisms in *Saccharomyces cerevisiae*. *Frontiers in Microbiol*. **11**, Article 582830; DOI: 10.3389/fmicb.2020.582830.
- 21. Philpott C.C., and Protchenko O. (2008) Response to Iron Deprivation in *Saccharomyces cerevisiae*. *Eukaryotic Cell*, 7, 20-27.
- 22. Outten C.E. and Albetel, A.N. (2013) Iron sensing and regulation in *Saccharomyces cerevisiae*: ironing out the mechanistic details. *Current Opinion in Microbiology* **16**, 662-668.
- 23. Courel, M., Lallet, S., Camadro, J.M., Blaiseau, P.L. (2005) Direct activation of genes involved in intracellular iron use by the yeast iron-responsive transcription factor Aft2 without its paralog Aft1. *Mol. Cell. Biol.* **25**, 6760-6771.
- 24. Portnoy, M.E., Jensen, L.T., Culotta, V.C. (2002) The distinct methods by which manganese and iron regulate the Nramp transporters in yeast. *Biochem. J.* **362**, 119-124.
- 25. Li L.T., Bagley, D., Ward, D.A., Kaplan, J. (2008) Yap5 is an iron-responsive

- transcriptional activator that regulates vacuolar iron storage in yeast. *Mol. Cell. Biol.* **28**, 1326-1337.
- 26. Puig, S., Vergara, S.V., Thiele, D.J. (2008) Cooperation of two mRNA-Binding proteins drives metabolic adaptation to iron deficiency. *Cell Metab.* 7, 555-564.
- 27. Rutherford, JC; Ojeda, L; Balk, J; Muhlenhoff, U; Lill, R; Winge, DR (2005) Activation of the iron regulon by the yeast Aft1/Aft2 transcription factors depends on mitochondrial but not cytosolic iron-sulfur protein biogenesis. *J. Biol. Chem.* **280**, 10135-10140.
- 28. Lill, R; Dutkiewicz, R; Freibert, SA.; Heidenreich, T; Mascarenhas, J; Netz, DJ.; Paul, VD.; Pierik, AJ.; Richter, N; Stuempfig, M; Srinivasan, V; Stehling, O; Mühlenhoff, U. (2015) The role of mitochondria and the CIA machinery in the maturation of cytosolic and nuclear iron-sulfur proteins. *Eur. J. Cell. Biol.* **94**, 280-291.
- 29. Kumanovics, A; Chen, OS.; Li, LT; Bagley, D; Adkins, EM; Lin, HL; Dingra, NN.; Outten, CE.; Keller, G; Winge, DR; Ward, DM.; Kaplan, J (2008) Identification of FRA1 and FRA2 as genes involved in regulating the yeast iron regulon in response to decreased mitochondrial iron-sulfur cluster synthesis. *J. Biol. Chem.* **283**, 10276-10286.
- 30. Bulteau, AL; Dancis, A; Gareil, M; Montagne, JJ; Camadro, JM; Lesuisse, E (2007) Oxidative stress and protease dysfunction in the yeast model of Friedreich ataxia. *Free Radical Biol. and Medicine* **42**, 1561-1570.
- 31. Miao R, Martinho M, Morales JG, Kim H, Ellis EA, Lill R, Hendrich, M.P., Münck, E., and Lindahl, P.A. (2008) EPR and Mössbauer spectroscopy of intact mitochondria isolated

- from Yah1p-depleted *Saccharomyces cerevisiae. Biochemistry* **47**, 9888–9899.
- 32. Zhang Y; Lyver ER.; Knight, SAB; Pain, D; Lesuisse, E; Dancis A (2006) Mrs3p, Mrs4p, and frataxin provide iron for Fe-S cluster synthesis in mitochondria. *J. Biol. Chem.* **281**, 22493-22502.
- 33. Miao R, Kim, H., Koppolu UMK, Ellis, E.A., Scott, R.A. and Lindahl, P.A. (2009) Biophysical characterization of the iron in mitochondria from Atm1-depleted Saccharomyces cerevisiae. Biochemistry 48, 9556-9568.
- 34. Duby, G; Foury, F; Ramazzotti, A; Herrmann, J.; Lutz, T (2002) A non-essential function for yeast frataxin in iron-sulfur cluster assembly. *Human Mol. Gen.* **11**, 2635-2643.
- 35. Wofford, J. D., and Lindahl, P. A. (2015) Mitochondrial iron sulfur-cluster activity and cytosolic iron regulate iron traffic in *Saccharomyces cerevisiae*. *J. Biol. Chem.* **290**, 26968–26977.
- 36. Wofford JD and Lindahl PA (2018) A Mathematical Model of Iron Import and Trafficking in WT and Mrs3/4ΔΔ Yeast Cells. *BMC Systems Biology*, **13**, Article 23; DOI: 10.1186/s12918-019-0702-2
- 37. Wofford, JD; Bolaji, N; Dziuba, N; Outten, FW; Lindahl PA (2019) Evidence that a respiratory shield in *Escherichia coli* protects a low molecular mass Fe^{II} pool from O₂-dependent oxidation. *J. Biol. Chem.*, 294, 50-62.
- 38. Park, J., McCormick, S.P., Chakrabarti M., and Lindahl P.A. (2013) Insights into the ironome and manganese-ome of Δmtm1 *Saccharomyces cerevisiae* mitochondria. *Metallomics*, **5**, 656-672.

- 39. Miao, R., Holmes-Hampton, G.P., and Lindahl P.A. (2011) Biophysical Investigation of the Iron in Aft1-lup and Gal-YAH1 Saccharomyces cerevisiae. Biochemistry **50**, 2660–2671
- 40. Foury, F; Roganti, T (2002) Deletion of the mitochondrial carrier genes MRS3 and MRS4 suppresses mitochondrial iron accumulation in a yeast frataxin-deficient strain. *J. Biol. Chem.* **277**, 24475-24483.
- 41. Seguin, A; Santos, R; Pain, D; Dancis, A; Camadro, J-M; Lesuisse, E (2011 Coprecipitation of Phosphate and Iron Limits Mitochondrial Phosphate Availability in *Saccharomyces cerevisiae* Lacking the Yeast Frataxin Homologue (YFH1). *J. Biol. Chem.* **286**, 6071-6079.
- 42. McNaughton, R. L., Reddi, A. R., Clement, M. H., Sharma, A., Barnese, K., Rosenfeld, L., Gralla, E. B., Valentine, J. S., Culotta, V. C., and Hoffman, B. M. (2010) Probing in vivo Mn2+ speciation and oxidative stress resistance in yeast cells with electron-nuclear double resonance spectroscopy. *Proc. Natl. Acad. Sci. U.S.A.* 107, 15335–15339.
- 43. Irazusta V., Cabiscol, E., Reverter-Branchat, G., Ros, J., Tamarit, J. (2006) Manganese is the link between frataxin and iron-sulfur deficiency in the yeast model of Friedreich ataxia. *J. Biol. Chem.* **281**, 12227-12232.
- 44. Kwast, KE; Lai, LC; Menda, N; James, DT; Aref, S; Burke, PV (2002) Genomic analyses of anaerobically induced genes in *Saccharomyces cerevisiae*: Functional roles of Rox1 and other factors in mediating the anoxic response. *J. Bacteriol.* **184**, 250-265.
- 45. Nguyen TQ, Dziuba, N., Lindahl, P.A. (2019) Isolated *Saccharomyces cerevisiae* vacuoles contain low-molecular-mass

- transition-metal polyphosphate complexes. *Metallomics*, **11**, 1298-1309.
- 46. Auchere, F., Santos, R., Planamente, S., Lesuisse, E., Camadro, J.-M. (2008) Glutathione-dependent redox status of frataxin-deficient cells in a yeast model of Friedreich's ataxia. *Human Mol. Gen.* 17, 2790-2802.
- 47. Park, J., McCormick S.P., Cockrell A.L., Chakrabarti, M., Lindahl, P.A. (2014) High-Spin Ferric ions in *Saccharomyces cerevisiae* vacuoles are reduced to the ferrous state during adenine-precursor detoxification. *Biochemistry*, **53**, 3940-3951.
- 48. Hudder, B.N., Garber-Morales J., Stubna, A.A., Münck E., Hendrich M,P., Lindahl, P.A. (2007) Electron paramagnetic resonance and Mössbauer spectroscopy of intact mitochondria from respiring *Saccharomyces cerevisiae*. *J. Biol. Inorg. Chem.* 12, 1029-1053.
- 49. Garber-Morales J., Holmes-Hampton, G.P., Miao, R., Guo, Y.S., Münck, E., Lindahl, P.A. (2010) Biophysical Characterization of Iron in Mitochondria Isolated from Respiring and Fermenting Yeast. *Biochemistry*, **49**, 5436-5444.
- 50. Holmes-Hampton G.P.; Miao R; Garber-Morales J., Guo Y.S., Münck, E., Lindahl, P.A., (2010) A Nonheme High-Spin Ferrous Pool in Mitochondria Isolated from Fermenting *Saccharomyces cerevisiae*. *Biochemistry*, **49**, 4227-4234.
- 51. Surovstev, I.V., Morgan, J.J., Lindahl, P.A. (2007) Whole-cell modeling framework in which biochemical dynamics impact aspects of cellular geometry. *J. Theor. Biol.* **244**, 154-166.
- 52. Babcock M., deSilva D., Oaks R., Davis-Kaplan S., Jiralerspong S., Montermini L.,

- Pandolfo M., and Kaplan J. (1997) Regulation of mitochondrial iron accumulation by Yfhl, a putative homolog of frataxin. *Science*, **276**, 1709-1 712.
- 53. Moreno-Cermeno, A., Obis E., Bellí G, Cabiscol E, Ros J. and Tamarit J. (2010) Frataxin Depletion in Yeast Triggers Upregulation of Iron Transport Systems before Affecting Iron-Sulfur Enzyme Activities. *J. Biol. Chem.* **285**, 41653-41664.
- 54. Ast, T., Meisel J.D., Patra, S., Wang, H., Grange, R.M.H., Kim S.H., Calvo, S.E., Orefice L.L., Nagashima F., Ichinose, F., Zapol W.M., Ruvkun G., Barondeau, D.P., Mootha, V.K. (2019) Hypoxia rescues frataxin loss by restoring iron sulfur cluster biogenesis. *Cell*, **177**, 1507-1521.
- 55. Pandey, A., Pain, J., Dziuba N., Pandey A.K., Dancis, A., Lindahl P.A., and Pain D. (2018) Mitochondria export sulfur species required for cytosolic tRNA thiolation. *Cell Chem. Biol.* **25**, 1-11.
- 56. Yoon, H., Zhang, Y., Pain, J., Lyver, ER., Lesuisse, E., Pain, D., Dancis, A. (2011) Rim2, a pyrimidine nucleotide exchanger, is needed for iron utilization in mitochondria. *Biochem. J.* **440**, 137-146.
- 57. Gao, C.Y., Pinkham, J.L. Tightly regulated beta-estradiol dose-dependent expression system for yeast" *Biotechniques* 2000, **29**, 1226-1231.
- 58. Kim, J.E., Vali, S.W., Nguyen, T.Q., Dancis, A., Lindahl, P.A. (2021) Mössbauer and LC-ICP-MS investigation of iron trafficking between vacuoles and mitochondria in vma2Δ *Saccharomyces cerevisiae*. *J. Biol. Chem.* **296**, 100141-100155.

FIGURE LEGENDS

Figure 1: Model describing iron trafficking and regulation in S. cerevisiae, with an emphasis on the cell's response to a decline in Yfh1 levels under aerobic vs hypoxic growth, and high vs low iron in the media. Blue region is cytosol, yellow is mitochondria, and green is vacuole. Points of regulation are indicated by red circles. The dashed red line emanates from the sensed species and terminates at the site of regulation. Regulation was "local"; FS (the iron regulon) regulates R_{cyt} , R_{vac} , and R_{23} ; FM (pool of Fe^{II} in mitochondria) regulates R_{mit} ; FC (labile iron pool in the cytosol) also regulates R_{vac} ; O2 regulates R_{isu} .

Figure 2: Western Blot of Yfh1 in crude mitochondria isolated from mutant cells grown on increasing concentrations of estradiol (in nM). Cells were grown on CSM under aerobic fermenting conditions and harvested at OD600 between 0.6 and 0.8. WT cells were grown in CSM hypoxic respiring conditions and harvested at a similar OD. 105 ug of protein were added to each well. Molecular masses of markers are given in kDa. aligned Markers are images using Seeblue TM prestained protein standard ladder; masses (in kDa) are indicated.

Figure 3: Mössbauer spectra of AFM cells with decreasing [EST] and [IRON] = 40. [EST] in nM was: A, 1000; B, 100; C, 50; D, 25; E, 10; F, 5; G, 2.5; H, 0. Red lines are composite simulations based on parameters in Table S2. Solid lines above A are simulations for nanoparticles (magenta), nonheme HS Fe^{II} (dark blue), heme HS Fe^{II} (light blue), the central doublet (green) and vacuolar Fe^{III} (brown). All MB spectra included in the paper were collected at ~ 5 K and 0.05 T, and with gamma radiation parallel to the field. Note scale differences between spectra. Pie charts the iron distribution corresponding spectra (as given in Table S2),

using the same color-coding as for the solid spectral line simulations.

Figure 4: EPR spectra of ERyfh1 cells grown in minimal media with different [EST] (in nM): Panel A: dashed line, AFM0-10; solid line, AFM2000-10; Panel B: red line AFM2000-10; blue line, HFM2000-10.

Figure 5: Mössbauer spectra of WT and Yfh1-deficient cells grown aerobically in media supplemented with different concentration of ⁵⁷Fe^{III} citrate. A, AFW-1; B, AFW-40; C, AFM0-1; D, AFM0-10; E, AFM0-100. The blue line in D is a simulation to HS Fe^{III} at 8% of spectral intensity.

Figure 6: Mössbauer spectra of fermenting cells grown in CSM under low O₂ conditions with no estradiol added. A, HFW-1; B, HFW-40; C, HFM0-1; D, HFM0-40.

Figure 7: Mössbauer spectra of respiring WT and Yfh1-deficient cells grown under aerobic and hypoxic ironsufficient conditions. A) ARW-40; B) HRW-40; C) ARM0-40; D) HRM0-40.

Figure 8: Mössbauer spectra of mitochondria isolated from hypoxic fermenting cells. A) HFW-1. B) HFW-40; C) HFM0-1; D) HFM0-40.

Figure 9: Mössbauer spectra of mitochondria isolated from hypoxic respiring cells. A) HRM0-40; B) HRW-40.

Figure 10. Simulations of MB-related species, given as a percentage of cellular iron, vs. nutrient iron concentration. Maroon, CD; Green, NHHS Fe^{III}; Blue, NHHS Fe^{III}; Red, nanoparticles. Nutrient IRON is plotted as log base 2 for better visualization.

Figure 11. Simulations of MB-related species, given as a percentage of cellular iron, vs. changes in the rate of ISC biosynthesis and O_2 . Top panel, % species vs. $k_{isu-max}$; rate for ΔY fh1 on left, rate for WT on right. Maroon, CD; Green, NHHS Fe^{III} ; Blue, NHHS Fe^{II} ; Red, MP nanoparticles (not combined with VP). Second and third panels, plots of aerobic \rightarrow hypoxic for WT-40 and ΔY fh1-40 cells. Red line is nanoparticles NP (MP plus VP), dashed red line is [O2], plotted on the right axis. Grey is FS. In the third panel, percent due to FS has been expanded 100-fold for better visualization.

Figure 1: Model describing iron trafficking and regulation in *S. cerevisiae*, with an emphasis on the cell's response to a decline in Yfh1 levels under aerobic vs hypoxic growth, and high vs low iron in the media. Blue region is cytosol, yellow is mitochondria, and green is vacuole. Points of regulation are indicated by red circles. The dashed red line emanates from the sensed species and terminates at the site of regulation. Regulation was "local"; FS (the iron regulon) regulates R_{cyt} , R_{vac} , and R_{23} ; FM (pool of Fe^{II} in mitochondria) regulates R_{mit} ; FC (labile iron pool in the cytosol) also regulates R_{vac} ; O2 regulates R_{tsu} .

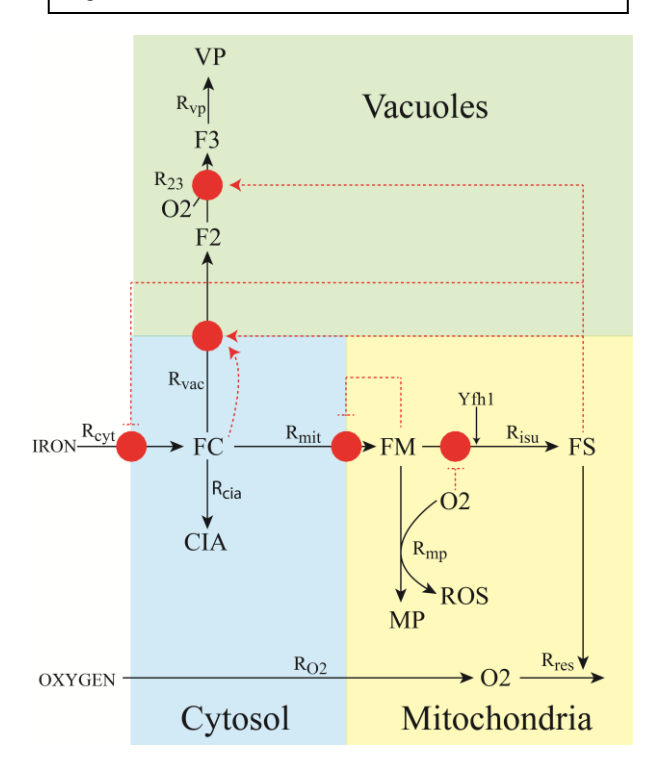


Figure 2: Western Blot of Yfh1 in crude mitochondria isolated from mutant cells grown on increasing concentrations of estradiol (in nM). Cells were grown on CSM under aerobic fermenting conditions and harvested at OD_{600} between 0.6 and 0.8. WT cells were grown in CSM hypoxic respiring conditions and harvested at a similar OD. 105 μ g of protein were added to each well. Molecular masses of markers are given in kDa. Markers are aligned images using Seeblue TM prestained protein standard ladder; masses (in kDa) are indicated.

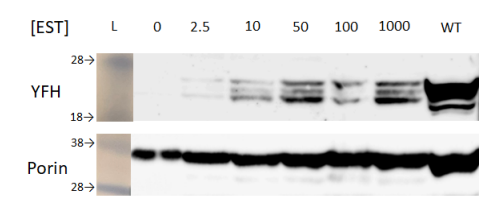


Figure 3: Mössbauer spectra of AFM cells with decreasing [EST] and [IRON] = 40. [EST] in nM was: A, 1000; B, 100; C, 50; D, 25; E, 10; F, 5; G, 2.5; H, 0. Red lines are composite simulations based on parameters in Table S2. Solid lines above A are simulations for nanoparticles (magenta), nonheme HS Fe^{II} (dark blue), heme HS Fe^{II} (light blue), the central doublet (green) and vacuolar Fe^{III} (brown). All MB spectra included in the paper were collected at ~ 5 K and 0.05 T, and with gamma radiation parallel to the field. Note scale differences between spectra. Pie charts show the iron distribution for the corresponding spectra (as given in Table S2), using the same color-coding as for the solid spectral line simulations.

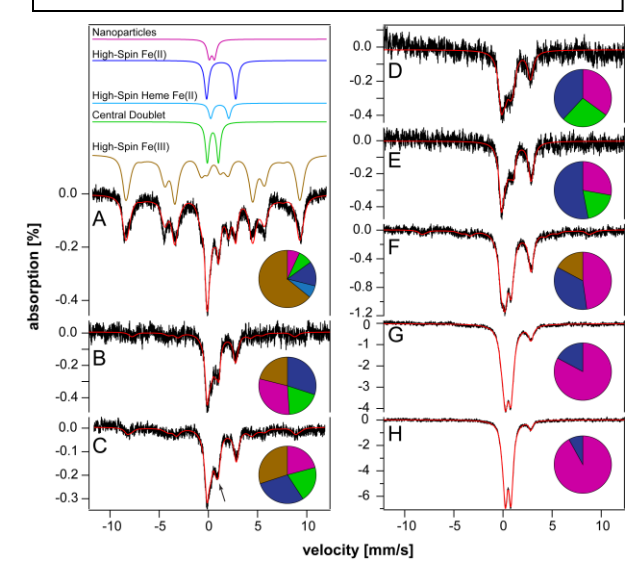


Figure 4: EPR spectra of ERyfh1 cells grown in minimal media with different [EST] (in nM): Panel A: dashed line, AFM0-10; solid line, AFM2000-10; Panel B: red line AFM2000-10; blue line, HFM2000-10.

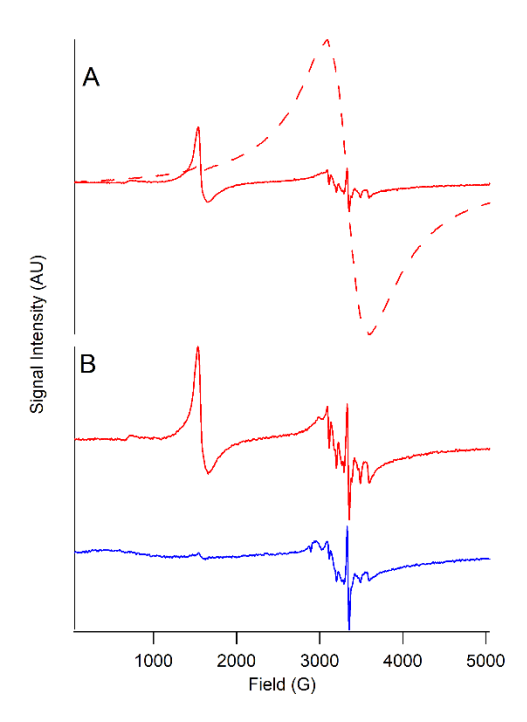


Figure 5: Mössbauer spectra of WT and Yfh1-deficient cells grown aerobically in media supplemented with different concentration of $^{57} Fe^{III}$ citrate. A, AFW-1; B, AFW-40; C, AFM0-1; D, AFM0-10; E, AFM0-100. The blue line in D is a simulation to HS Fe^{III} at 8% of spectral intensity.

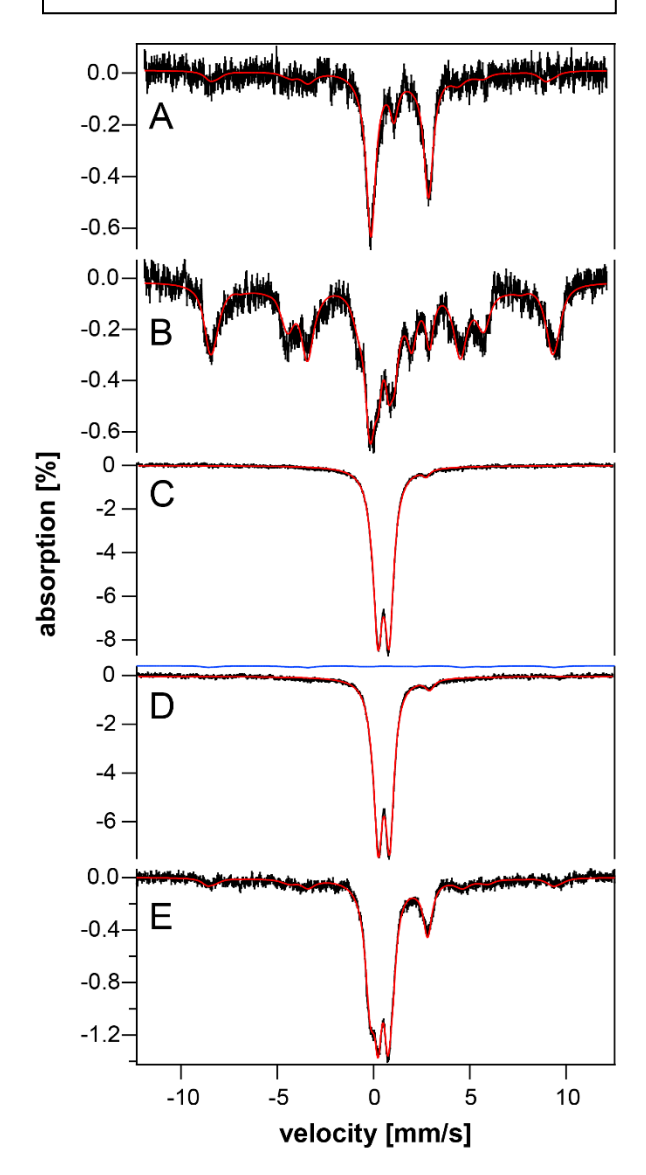


Figure 6: Mössbauer spectra of fermenting cells grown in CSM under low O₂ conditions with no estradiol added. A, HFW-1; B, HFW-40; C, HFM0-1; D, HFM0-40.

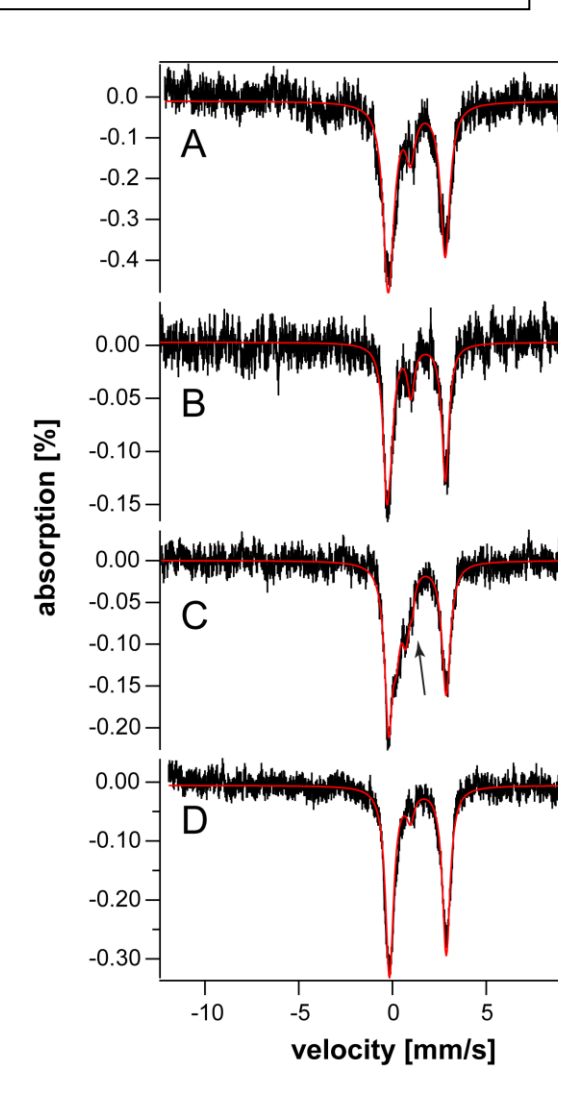


Figure 7: Mössbauer spectra of respiring WT and Yfh1-deficient cells grown under aerobic and hypoxic iron-sufficient conditions. A) ARW-40; B) HRW-40; C) ARM0-40; D) HRM0-40.

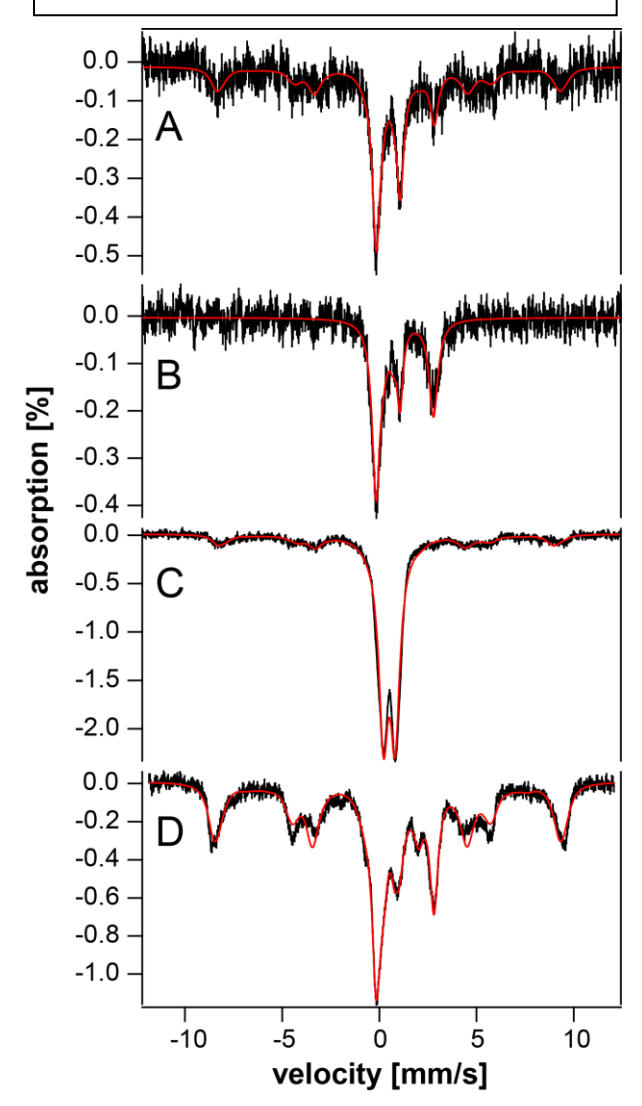


Figure 8: Mössbauer spectra of mitochondria isolated from hypoxic fermenting cells. A) HFW-1. B) HFW-40; C) HFM0-1; D) HFM0-40.

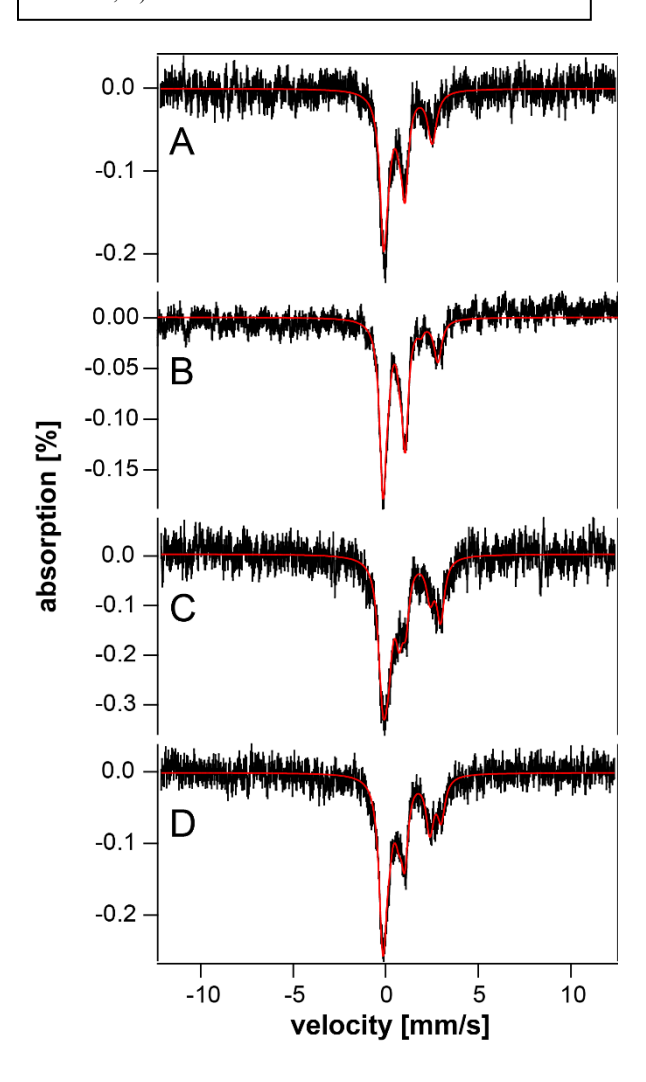


Figure 9: Mössbauer spectra of mitochondria isolated from hypoxic respiring cells. A) HRM0-40; B) HRW-40.

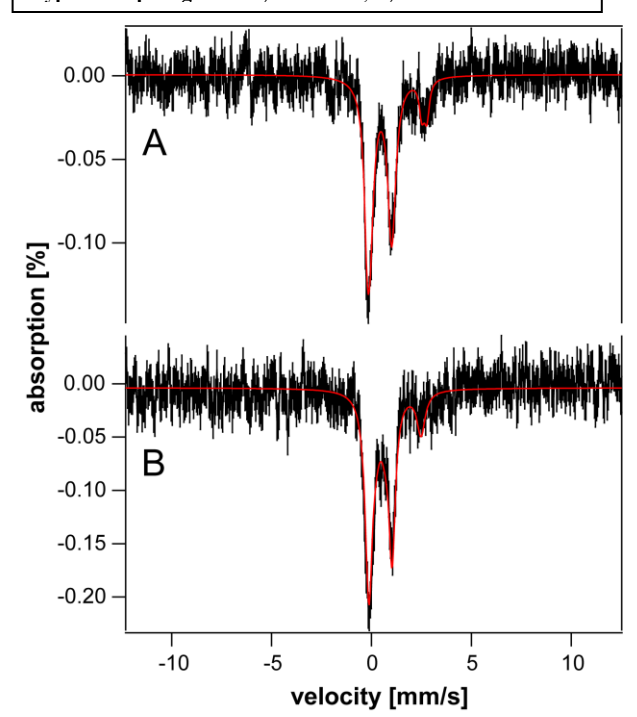


Figure 10. Simulations of MB-related species, given as a percentage of cellular iron, vs. nutrient iron concentration. Maroon, CD; Green, NHHS Fe^{III}; Blue, NHHS Fe^{III}; Red, nanoparticles. Nutrient IRON is plotted as log base 2 for better visualization.

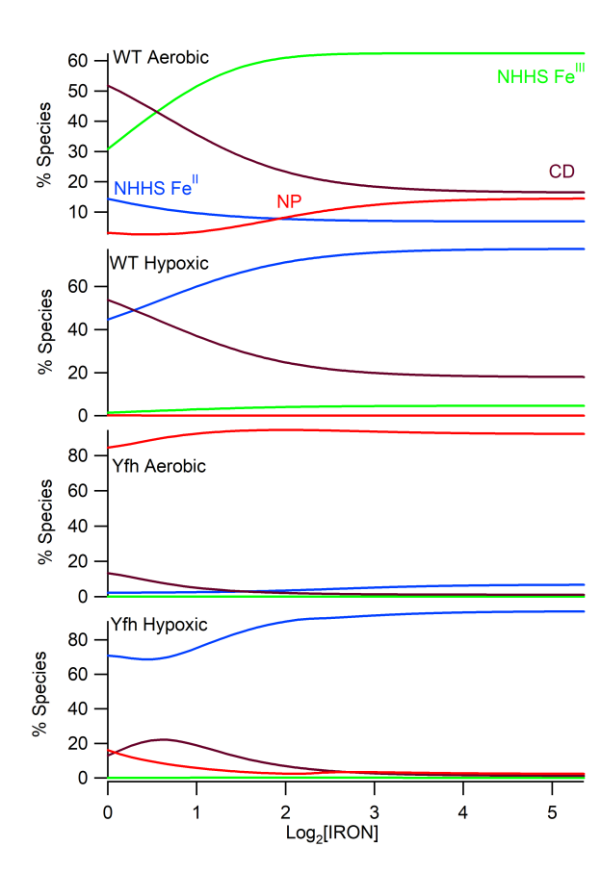


Figure 11. Simulations of MB-related species, given as a percentage of cellular iron, vs. changes in the rate of ISC biosynthesis and O_2 . Top panel, % species vs. $k_{isu-max}$; rate for Δ Yfh1 on left, rate for WT on right. Maroon, CD; Green, NHHS Fe^{III} ; Blue, NHHS Fe^{II} ; Red, MP nanoparticles (not combined with VP). Second and third panels, plots of aerobic \rightarrow hypoxic for WT-40 and Δ Yfh1-40 cells. Red line is nanoparticles NP (MP plus VP), dashed red line is [O2], plotted on the right axis. Grey is FS. In the third panel, percent due to FS has been expanded 100-fold for better visualization.

